Structure, Magnetism, and Properties of Ruddlesden−Popper Calcium Manganates Prepared from Citrate Gels

Ian D. Fawcett, Joseph E. Sunstrom IV, and Martha Greenblatt*

Department of Chemistry, Rutgers, The State University of New Jersey, Piscataway, New Jersey 08854

Mark Croft

Department of Physics, Rutgers, The State University of New Jersey, Piscataway, New Jersey 08855

K. V. Ramanujachary

Department of Chemistry and Physics, Rowan University of New Jersey, Glassboro, New Jersey 08028

Received May 28, 1998. Revised Manuscript Received August 10, 1998

Ruddlesden−Popper (RP) phases with the formula $(CaO)(CaMnO_3)_n$, where $n = 1$, 2, 3, and ∞, have been prepared using the Pechini citrate gel process at temperatures as low as 900 °C under flowing oxygen. The compounds were characterized by X-ray powder diffraction, Rietveld profile analysis, thermal gravimetric analysis, iodometric titrations, Mn K-edge X-ray absorption spectroscopy, temperature-dependent magnetic susceptibility, and resistivity. Rietveld analysis shows that there is an elongation in the apical Mn−O distances of the MnO_6 octahedra, which increases with decreasing dimensionality. Mn K-edge X-ray absorption spectroscopy and iodometric titrations show no detectable amount of Mn^{3+} (a Jahn−Teller distorted d^4 ion) in the samples indicating that the MnO_6 deformation may be associated with a splitting in the half-filled t_{2g} levels of Mn^{4+}. Magnetic susceptibility measurements show spontaneous magnetic ordering to antiferromagnetic states at ∼125 K for $CaMnO_3$ and $Ca_4Mn_3O_{10}$ and at ∼110 K for Ca_2MnO_4 and $Ca_3Mn_2O_7$. The effective magnetic moment is greatly suppressed in all of the RP manganates, even in the three-dimensional $CaMnO_3$, $n = \infty$ phase, and decreases dramatically with decreasing dimensionality. Large deviations from Curie−Weiss behavior are observed above the ordering temperature, which increase with decreasing n. These observations are discussed in terms of two-dimensional magnetic fluctuations and alternative mechanisms. The compounds are all poor electronic conductors with room-temperature resistivities in the range of 10^2−10^4 Ω cm.

Introduction

Since the discovery of a large magnetoresistance effect in $La_{1-x}A_xMnO_3$ (A = divalent cation),[1] a significant research effort has been directed toward the synthesis and characterization of new compounds, particularly manganates, which exhibit giant magnetoresistance (GMR) or colossal magnetoresistance (CMR).[2] The impetus for such an effort lies in the vast potential in revolutionizing our existing magnetic storage and retrieval technologies.[3,4] Despite the amount of research being conducted in this area, the GMR−CMR phenomena are still poorly understood.

It has been suggested that a double-exchange mechanism is responsible for the coexistence of ferromagnetic and metallic properties in manganate perovskites.[5] This double-exchange mechanism requires mixed-valent manganese (Mn^{3+}, Mn^{4+}) to be present as in the case of $La_{1-x}Sr_xMnO_3$. However, recent reports on the observation of GMR effects in the pyrochlore $Tl_2Mn_2O_7$[6,7] (with manganese exclusively in its tetravalent state) could not be rationalized on the double-exchange model. Clearly,

* To whom correspondence should be addressed. Phone: 732-445-3277. Fax: 732-445-5312. E-mail: martha@rutchem.rutgers.edu.

(1) McCormack, M.; Jin, S.; Tiefel, T.; Fleming, R. M.; Phillips, J. M.; Ramesh, R. *Appl. Phys. Lett.* **1994**, *64*, 3045.
(2) Rao, C. N. R.; Cheetham, A. K.; Mahesh, R. *Chem. Mater.* **1996**, *8*, 2421.
(3) von Helmolt, R.; Holzapfel, B.; Schultz, L.; Samwer, K. *Phys. Rev. Lett.* **1994**, *71*, 2331.
(4) Jin, S.; Tiefel, T. H.; McCormack, M.; Fastnacht, R. A.; Ramesh, R.; Chen, L. H.*Science* **1994**, *264*, 413.
(5) Zener, C. Phys. Rev. **1951**, *82*, 403. Anderson, P. W.; Hasegawa, H. *Phys. Rev.* **1955**, *100*, 675. de Gennes, P.-G. *Phys. Rev.* **1960**, *118*, 141. Millis, A. J.; Littlewood,; P. B.; Shraiman, B. I. *Phys. Rev. Lett.* **1995**, *74*, 5144; **1996**, *B53*, 8434. Goodenough, J. B. *Phys. Rev.* **1976**, *164*, 785.
(6) Subramanian, M. A.; Toby, B. H.; Ramirez, A. P.; Marshall, W. J.; Sleight, A. W.; Kwei, G. H. *Science* **1996**, *273*, 81.
(7) Rosenfeld, H. D.; Subramanian, M. A. *J. Solid State Chem.* **1996**, *125*, 278.

10.1021/cm980380b CCC: $15.00
Published on Web 10/09/1998

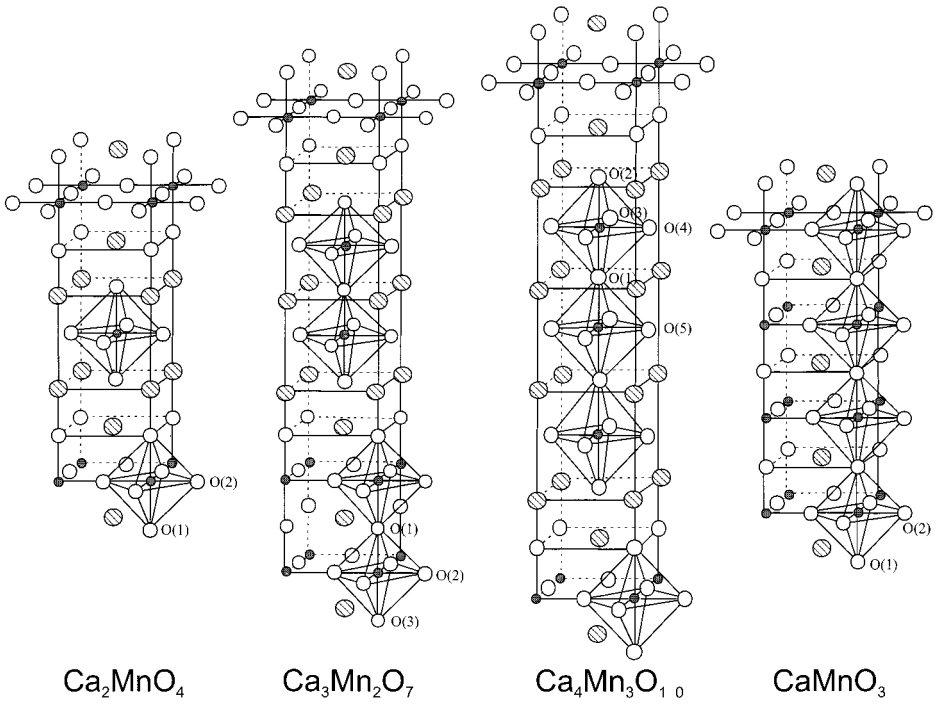

Figure 1. Structural representation of the Ruddlesden−Popper series, where A = Ca and B = Mn in this case.

the importance of mixed-valency and crystal structure in manganates with GMR properties is not well understood.

As part of our current efforts in understanding the evolution of electronic properties as a function of mixed-valency and dimensionality, we have undertaken a detailed examination of the structure and electronic properties of the Ruddlesden−Popper (RP) phases $(CaO)(CaMnO_3)_n$ (n = 1, 2, 3, ∞).[8−11] Figure 1 shows the structures of the RP phases for n = 1, 2, 3, and ∞ (from left to right). The n = ∞ and n = 1 compounds ($CaMnO_3$ and Ca_2MnO_4, respectively) can be considered as the end-members of the RP series. The n = ∞ compound has a perovskite-type structure, characterized by a three-dimensional (3D) array of corner sharing MnO_6 octahedra. The n = 1 compound forms with the two-dimensional (2D) K_2NiF_4-type structure with $CaMnO_3$ perovskite layers alternating with CaO rock salt layers. In the n = 2 ($Ca_3Mn_2O_7$) and n = 3 ($Ca_4Mn_3O_{10}$) compounds two and three $CaMnO_3$ perovskite layers are interconnected by corner-sharing MnO_6 octahedra, respectively. One of the important aspects of this series is that manganese remains tetravalent for all values of n; therefore, the electrical and magnetic properties can be studied as a function of dimensionality (i.e. n) while the formal valence of manganese remains fixed at 4+.

The entire RP series of calcium manganates has previously been prepared but at high oxygen pressure.[12] In addition, the magnetic properties of the compounds synthesized by high oxygen pressure have been studied.[12−14] A recent structural and magnetic properties study of the $Ca_4Mn_3O_{10}$ suggested it to be a new GMR material.[13] More recently Battle et al. showed that $Ca_4Mn_3O_{10}$ orders spontaneously at 115 K most likely with a G-type antiferromagnetic ordering.[14]

This paper details the synthesis and characterization of $(CaO)(CaMnO_3)_n$ (n = 1, 2, 3, ∞) materials prepared by the Pechini citrate gel technique.[15] This study is published as part 1 of a systematic study of the relationship of valence and structural dimensionality to magnetoresistance phenomena in RP manganates.

Experimental Section

Synthesis. All starting materials were a minimum of reagent grade purity. The molecular weight of $Ca(NO_3)_2{\cdot}4H_2O$ (Aldrich, 99+%) was checked immediately before reaction by decomposition to CaO with a TA Instruments thermal gravimetric analyzer (model 2050). $Mn(NO_3)_2$ (Aldrich) was purchased as a 49.7% w/w aqueous solution. To prepare the calcium manganates, appropriate stoichiometry of metal nitrates were dissolved in 25 mL of distilled water. An excess of citric acid (Aldrich, 99.5+%) and ethylene glycol (Aldrich, 99+%) was added, and the mixture was stirred mechanically for 10−15 min. Several drops of concentrated nitric acid were added to prevent precipitation of $Ca(OH)_2$. The mixture was then slowly heated on a hot plate to remove the water and form a gel. **Care should be exercised at this step, as the addition of too much nitric acid could result in self-ignition of the mixture.** The gel was then placed in a furnace and heated slowly to 500 °C to decompose the nitrates and ignite the carbonaceous material. The decomposed gel was removed from the furnace when the resultant ash stopped glowing. The ash was then ground and pressed into pellets using a $^1/_2$-in. diameter die under a pressure of 7000 psi. The pellets were then fired at 1200 °C in flowing oxygen for 12 h.

$LaMnO_3$ and $LaCaMnO_4$ were synthesized for the Mn K-edge X-ray absorption spectroscopy (XAS) measurements

(8) Wollan, E. O.; Koehler, W. C. *Phys. Rev.* **1955**, *100*, 545.
(9) Ruddlesden, S. N.; Popper, D. *Acta Crystallogr.* **1951**, *10*, 538. Brisi, C.; Lucco-Borlera, M. *Atti. Acad. Sci. Torino* **1961−62**, *96*, 805.
(10) Brisi, C. *Ann. Chem.* **1961**, *51*, 1399.
(11) Brisi, C.; Lucco-Borlera, M. *J. Inorg. Nucl. Chem.* **1965**, *27*, 2129.
(12) MacChesney, J. B.; Williams, H. J.; Potter, J. F.; Sherwood, R. C. *Phys. Rev.* **1967**, *164 (2)*, 779.
(13) Rossell, H. J.; Goodman, P.; Bulcock, S.; March, R. H. S.; Kennedy, J.; White, T.; Lincoln, F. J.; Murray, K. S. *Aust. J. Chem.* **1996**, *49*, 205.
(14) Battle, P. D.; Green, M. A.; Lago, J.; Millburn, J. E.; Rosseinsky, M. J.; Vente, J. F. *Chem. Mater.* **1998**, *10*, 658.
(15) Pechini, M. U.S. Patent No. 3,330,697, July 1967.

Table 1. Lattice Parameters for the Calcium Manganate RP Phases

compd	*a* (Å)	*b* (Å)	*c* (Å)	space group	Mn valence[a]
Ca_2MnO_4[b]	5.18334(5) (5.183(1))		24.1023(5) (24.117(4))	$I4_1/acd$	4.0
$Ca_3Mn_2O_7$[c]	3.68338(8) (3.71)		19.5748(8) (19.50)	$I4/mmm$	3.96
$Ca_4Mn_3O_{10}$[d]	5.2492(5) (5.26557(12))	5.2407(5) (5.26039(11))	27.119(2) (26.8276(5))	$Pbca$	4.02
$CaMnO_3$[e]	5.2770(2) (5.279(1))	7.4510(4) (7.448(1))	5.2643(2) (5.264(1))	$Pnma$	3.96

[a] From iodometric titration; error is ±0.01. Values of the lattice parameters in parentheses were taken from the following: [b]ref 21; [c]ref 10; [d]ref 14; [e]ref 20.

(see below). Stoichiometric quantities of La_2O_3 (Cerac, 99.99%, dried in air at 800 °C), $Mn(NO_3)_2$ (and $Ca(NO_3)_2{\cdot}4H_2O$ for $LaCaMnO_4$) were dissolved in a minimum (typically 50 mL) of dilute (∼2 M) nitric acid to which citric acid and ethylene glycol were added. The solution was heated on a hot plate to give a gel which was decomposed to a powder by further heating to 500 °C as described above. To prepare $LaCaMnO_4$, the resultant powder was heated at 1200 °C under flowing O_2 for 12 h. $LaMnO_3$ was prepared by firing the powder in air at 1100 °C for 12 h, followed by heating under flowing Ar at 1200 °C for 12 h.

Thermal gravimetric analysis (TGA) of the product was carried out on approximately 10−15 mg of sample, which was placed on a platinum pan and heated to 950 °C at 10 °C/min in flowing N_2 or O_2 (50 cm^3/min). The oxidation state of manganese was determined by iodometric titration employing an amperometric dead-stop end-point detection, using the technique described by Licci et al.[16]

X-ray Absorption Spectroscopy (XAS). The Mn K-edge XAS measurements were performed on beam line X-19A at the Brookhaven National Synchrotron Light Source using a double crystal Si(311) monochromator. Electron yield, fluorescence mode,[17] and transmission mode measurements were made and all were checked for consistency. A standard was run simultaneously with all measurements for precise calibration. The relative energies between various spectra were established by careful comparison of the standard spectra. Particular care was taken to use the identical standard sample maintained in a constant position to accurately calibrate the chemical shift results. In general, the relative accuracy of the energy is about ±0.05 eV. The absolute energy of the spectra is pinned to the first inflection point of pure Mn (6539.0 eV) and to the main peak of MnO (6555.0 eV). All spectra were normalized to unity step in the absorption coefficient from well below to well above the edge.

Powder X-ray diffraction (PXD) was obtained with a Scintag PAD V diffractometer with monochromatized Cu Kα radiation and a liquid-nitrogen-cooled Li-drifted germanium detector. Samples were ground with silicon as the internal standard and placed on glass slides with petroleum jelly. Lattice parameters were refined with a least-squares fitting program. In addition, Rietveld profile fitting[18] of the room-temperature PXD data was completed using the program GSAS.[19]

Magnetic Susceptibility (χ). Temperature-dependent χ measurements were obtained using a Quantum Design SQUID magnetometer (MPMS) over the temperature range 10−350 K in an applied field of 15 000 G.

Electrical resistivity (ρ) measurements as a function of temperature were made with a standard four-probe method in an APD Cryogenics closed-cycle helium refrigerator. Ultrasonically drawn indium wires were attached to sintered polycrystalline samples, with silver paint.

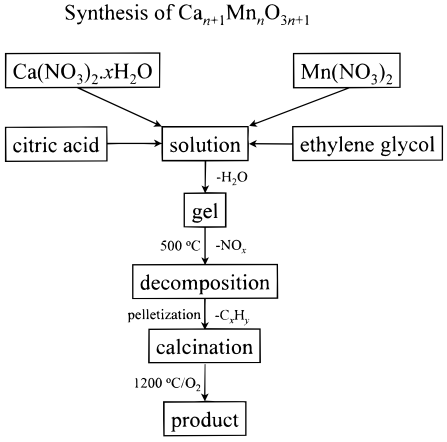

Figure 2. Schematic representation of the synthetic method used in this study.

Results

Synthesis. Pure phase samples of the $(CaO)(CaMnO_3)_n$ (n = 1, 2, 3, ∞) series have been prepared using the Pechini gel method[15] as summarized schematically in Figure 2. Although phase formation occurs as low as ∼900 °C, the crystallinity of the phases greatly improved when heat treated at 1100−1200 °C. All samples in this study showed neither gain nor loss of weight up to 1000 °C in O_2 or N_2 atmospheres. Iodometric titrations confirmed that all the calcium manganate samples contained manganese in the 4+ oxidation state (Table 1).

Structure. The PXD data, refined profiles, and difference plots for Ca_2MnO_4, $Ca_3Mn_2O_7$, $Ca_4Mn_3O_{10}$, and $CaMnO_3$ are shown in Figures 3. The lattice parameters, summarized in Table 1, are consistent with earlier data,[12,14,20,21] except for those of the $n = 3$ phase (to be discussed latter). The backgrounds of the PXD data in the Rietveld refinements were fitted with an 8-term Chebyshev polynomial, and a pseudo-Voigt function was employed to model the peak shapes. The initial positional parameters for $CaMnO_3$, Ca_2MnO_4, and $Ca_4Mn_3O_{10}$ were taken from previous studies.[14,20,21] For $Ca_3Mn_2O_7$, the initial parameters were taken from the study of $Sr_3Ti_2O_7$.[22] In the case of $CaMnO_3$, $Ca_3Mn_2O_7$, and $Ca_4Mn_3O_{10}$, physically sensible isotropic temperature factors could not be refined and so the values were fixed at 0.01 $Å^2$ in the final refinements. The parameters obtained after the refinements converged are listed in Tables 2−5. The Mn−O distances and Mn−O−Mn angles for the series are shown in Table 6. There are two distinct Mn−O distances for $CaMnO_3$ which show

(16) Licci, F.; Turilli G.; Ferro, P. *J. Magn. Magn. Mater.* **1996**, *164*, L268.
(17) Guo, T.; denBoer, M. *Phys. Rev.* **1984**, *B31*, 6233 Guo, T.; denBoer, M. *X-ray Absorption: Principles, Applications, Techniques of EXAFS and SEXAFS, and XANES*; Koningsberger, D., Reins, R., Eds.; Wiley: New York, 1988.
(18) Rietveld, H. M. *Acta Crystallogr.* **1967**, *22*, 151. Rietveld, H. M. *J. Appl. Crystallogr.* **1969**, *2*, 65.
(19) Larson, A. C.; von Dreele, R. B. *GSAS-Generalized Crystal Structure Analysis System*; Report No. LA-UR-86-748; Los Alamos National Laboratory: Los Alamos, NM, 1987.
(20) Poeppelmeier, K. R.; Leonowicz, M. E.; J. C. Scanlon, M. E.; Longo, J. M.; Yelon, W. B. *J. Solid State Chem.* **1982**, *45*, 71.
(21) Leonowicz, M. E.; Poeppelmeier, K. R.; Longo, J. M. *J. Solid State Chem.* **1985**, *59*, 71.
(22) Ruddlesden, S. N.; Popper, P. *Acta Crystallogr.* **1958**, *11*, 54.

Table 2. Atomic Parameters for $CaMnO_3$ Refined in the Space Group *Pnma*[a]

atom	site	*x*	*y*	*z*
Ca	4c	0.0272(9)	0.25	−0.007(2)
Mn	4b	0	0	0.5
O(1)	4c	0.487(3)	0.25	0.085(4)
O(2)	8d	0.289(3)	0.023(3)	−0.289(3)

[a] $R_p = 1.96\%$, $R_{wp} = 2.47\%$, and $\chi^2 = 1.26$ for 7499 observations and 23 variables.

Table 3. Atomic Parameters for Ca_2MnO_4 Refined in the Space Group *I*4$_1$/*acd*[a]

atom	site	*x*	*y*	*z*	$100U_{iso}$ (Å^2)
Ca	16d	0	0.25	0.55095(9)	0.3(1)
Mn	8a	0	0.25	0.375	1.0(1)
O(1)	16d	0	0.25	0.4600(3)	0.7(1)
O(2)	16f	0.215(1)	0.465(1)	0.125	1.5(3)

[a] $R_p = 2.96\%$, $R_{wp} = 3.77\%$, and $\chi^2 = 1.345$ for 7499 observations and 22 variables.

Table 4. Atomic Parameters for $Ca_3Mn_2O_7$ Refined in the Space Group *I*4/*mmm*[a]

atom	site	*x*	*y*	*z*
Ca(1)	2b	0	0	0.5
Ca(2)	4e	0	0	0.3114(2)
Mn	4e	0	0	0.0977(3)
O(1)	2a	0	0	0
O(2)	8g	0	0.5	0.0871(5)
O(3)	4e	0	0	0.2047(8)

[a] $R_p = 2.79\%$, $R_{wp} = 3.92\%$, and $\chi^2 = 2.679$ for 7499 observations and 19 variables.

Table 5. Atomic Parameters for $Ca_4Mn_3O_{10}$ Refined in the Space Group *Pbca*[a]

atom	site	*x*	*y*	*z*
Ca(1)	8c	0.502(6)	0.499(8)	0.0710(4)
Ca(2)	8c	−0.003(5)	−0.009(11)	0.2072(3)
Mn(1)	4b	0	0.5	0
Mn(2)	8c	0.505(5)	−0.005(8)	0.1380(3)
O(1)	8c	0.490(16)	0.007(13)	0.068(1)
O(2)	8c	0.510(12)	−0.007(13)	0.2272(8)
O(3)	8c	0.807(9)	0.211(4)	0.119(1)
O(4)	8c	0.210(13)	0.789(4)	0.152(1)
O(5)	8c	0.293(13)	0.289(4)	−0.006(2)

[a] $R_p = 1.91\%$, $R_{wp} = 2.92\%$, and $\chi^2 = 4.561$ for 7999 observations and 37 variables.

little variation from each other (1.89(2) and 1.919(5) Å). The bond angles for $CaMnO_3$ deviate just slightly from 90 and 180°, which is in agreement with the results of a previous single-crystal structure analysis.[21] With decreasing dimensionality, there is increasing distortion in the MnO_6 octahedra characterized by a lengthening of the bond between manganese and the apical oxygens. The Mn−O bond distances for the other end-member, Ca_2MnO_4, are 1.849(2) and 2.046(6) Å. The $Ca_3Mn_2O_7$ structure has three distinct bond distances (1.853(1), 1.918(6), 2.09(2) Å) with the longest distance again between the manganese and apical oxygen atoms. There are nine distinct Mn−O distances in $Ca_4Mn_3O_{10}$ which vary from 1.84(3) to 2.42(2) Å. It should be noted that while the positions of oxygen obtained from powder X-ray diffraction studies are not generally very reliable in an absolute sense, they can be used with some confidence to analyze trends in bond distances and bond angles.

XAS. Figure 4 shows a comparison of the Mn K-edge X-ray absorption spectra of the RP phases $(CaO)(CaMnO_3)_n$ or $Ca_{n+1}Mn_nO_{3n+1}$ ($n = 1$, 2, 3, and ∞), the formally Mn^{3+} and Mn^{4+} perovskites ($n = \infty$) $LaMnO_3$ and $CaMnO_3$, respectively, and the $n = 1$ RP phases $LaCaMnO_4$ and Ca_2MnO_4. In Figure 4 the preedge a feature, near 6545 eV, should be noted in all of the spectra. Figure 5 shows the preedge a features for $LaMnO_3$, $CaMnO_3$, $LaCaMnO_4$, and Ca_2MnO_4. In Figure 6, the preedge regions of the four RP calcium manganates studied in this paper are displayed.

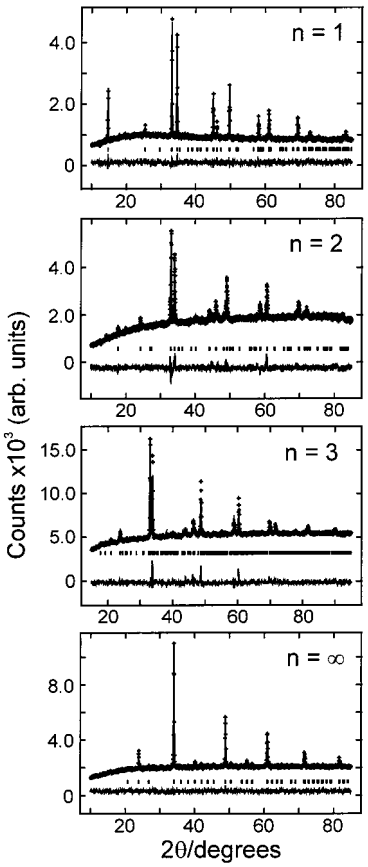

Figure 3. Observed (+) and calculated (solid line) X-ray diffraction patterns for (from top): Ca_2MnO_4, $Ca_3Mn_2O_7$, $Ca_4Mn_3O_{10}$, and $CaMnO_3$. The difference plot is located at the bottom of each figure. Tic marks represent allowed reflections.

Table 6. Mn−O Bond Distances (Å) and Mn−O−Mn Bond Angles (deg) for the Calcium Manganate RP Phases

	$CaMnO_3$		
Mn−O(1) ×2	1.919(5)	Mn−O(1)−Mn	152(1)
Mn−O(2) ×4	1.89(2)	Mn−O(2)−Mn	159.6(8)
	Ca_2MnO_4		
Mn−O(1) ×2	2.046(6)	Mn−O(2)−Mn	164.8(7)
Mn−O(2) ×4	1.849(2)		
	$Ca_3Mn_2O_7$		
Mn−O(1)	1.918(6)	Mn−O(1)−Mn	180
Mn−O(2) ×4	1.853(1)	Mn−O(2)−Mn	167.5(8)
Mn−O(3)	2.09(2)		
	$Ca_4Mn_3O_{10}$		
Mn(1)−O(1) ×2	1.84(3)	Mn(1)−O(5)−Mn(1)	159(3)
Mn(1)−O(5) ×2	1.87(5)	Mn(1)−O(1)−Mn(2)	175(5)
Mn(1)−O(5) ×2	1.90(6)	Mn(2)−O(3)−Mn(2)	142(2)
Mn(2)−O(1)	1.91(3)	Mn(2)−O(4)−Mn(2)	151(3)
Mn(2)−O(2)	2.42(2)		
Mn(2)−O(3)	1.86(4)		
Mn(2)−O(3)	2.02(5)		
Mn(2)−O(4)	1.92(6)		
Mn(2)−O(4)	1.94(6)		

Magnetic Susceptibility. Figure 7 shows the molar magnetic susceptibility (χ_M) vs temperature plots for

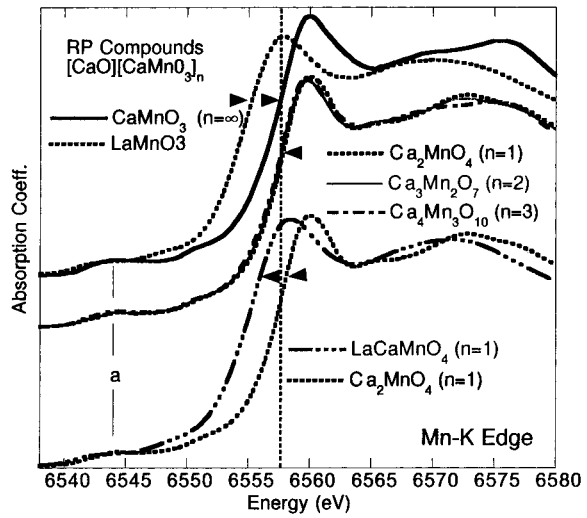

Figure 4. Comparison of the Mn K-edge spectra of the RP phase $(CaO)(CaMnO_3)_n$ ($n = 1$, 2, 3, and ∞) or $Ca_{n+1}Mn_nO_{3n+1}$ compounds, the formally Mn^{3+}/Mn^{4+} perovskite ($n = \infty$, RP) $LaMnO_3/CaMnO_3$ compounds, and the $n = 1$, RP Ca_2MnO_4/$LaCaMnO_4$ compounds.

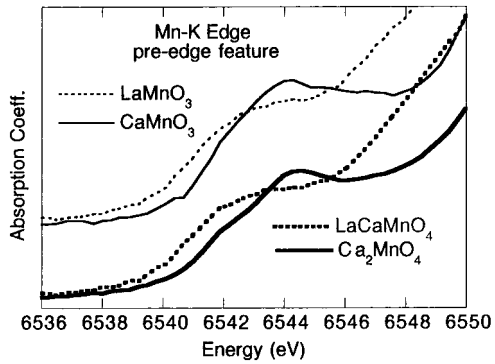

Figure 5. The preedge a features for the pure Ca and La substituted $n = 1$ and $n = \infty$ RP phases. The level of La substitution generates formally Mn^{3+} from the initially formal Mn^{4+} RP compounds. Note the very similar decrease in the a feature (d final state related) spectral weight consistent with a strong d character of the La-doped electrons.

$CaMnO_3$, $Ca_4Mn_3O_{10}$, $Ca_3Mn_2O_7$, and Ca_2MnO_4. The magnetization measurements were made in a field of 15 000 G, similar to the measurements made by MacChesney et al.[12] The results are discussed in terms of the magnetic susceptibility $\chi = M/H$. In the ordered phases, the 15 000 G field yields results which could, in principle, differ from the low-field limit of the susceptibility if the spin canting in the antiferromagnetic phases is nonlinear. All of the susceptibility results have been reduced to the units of emu/mol of Mn so that the Mn magnetic response between the various systems can be compared directly. All of the compounds show magnetic ordering. The $CaMnO_3$ ($n = \infty$) and $Ca_4Mn_3O_{10}$ ($n = 3$) ordering temperatures (both about 125 K) can be identified by the inflection in the $M(T)/H$ vs T curves, while $Ca_3Mn_2O_7$ ($n = 2$) and Ca_2MnO_4 ($n = 1$) show antiferromagnetic ordering at ~110 K. In Figure 8 an expanded view of the $T > T_N$ range of Figure 7 is presented. Figure 9 shows the temperature dependence of the reciprocal susceptibility, χ^{-1}, for all the RP phases studied here; the dashed line in the figure indicate the Curie−Weiss law (CW) behavior.

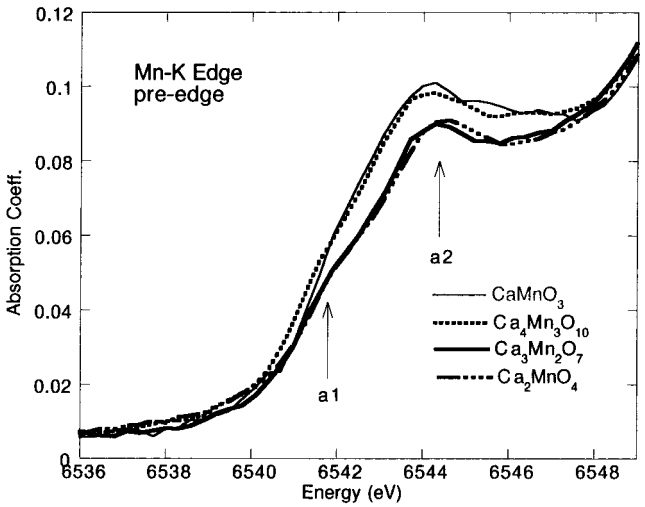

Figure 6. The preedge regions of the RP phase $(CaO)(CaMnO_3)_n$ ($n = 1$, 2, 3, and ∞). In this expanded view it is clear that there is an unresolved bimodal character to this feature with the two components being labeled by a1 and a2. This splitting is strongest for the $n = 1$ material and weakens progressively in the $n = 2$, $n = 3$, and $n = \infty$.

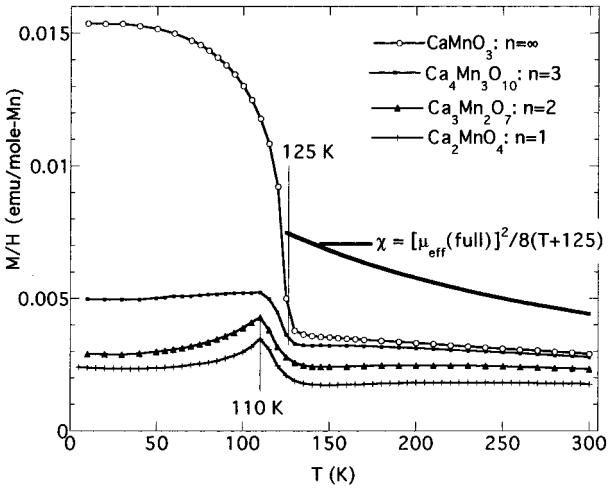

Figure 7. Magnetic susceptibility $\chi = M/H$ for the $(CaO)(CaMnO_3)_n$ ($n = 1$, 2, 3, and ∞) RP phases studied in this work.

Electrical Resistivity. All samples in the series have high room-temperature resistivities varying from $\sim 10^2$ to 10^4 Ω cm. Figure 10 shows the natural log of the resistivity ($\ln(\rho)$) plotted as a function of reciprocal temperature for $Ca_{n+1}Mn_nO_{3n+1}$ ($n = 1$, 2, 3, and ∞). In Table 7 the gap energy (Δ), the room-temperature resistivity (ρ_{RT}), and the preexponetial factor (ρ_0) are summarized.

Discussion

Synthesis. The Pechini method offers several advantages in this system. First, the citrate gel method coupled with careful analysis of starting reagents allows careful control over product stoichiometry. The method also allows the synthesis of materials at lower processing temperatures and with smaller particle sizes. The materials prepared in this study could be formed at temperatures as low as 900 °C. Most importantly, the method allowed the preparation of the materials at ambient oxygen pressures which is an inherent advantage of the smaller particle size.

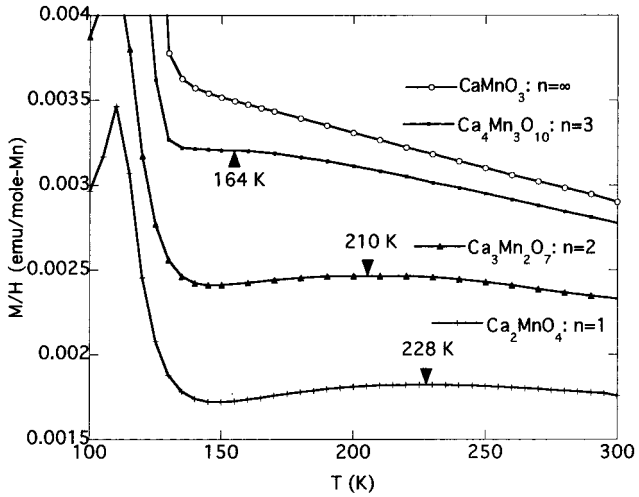

Figure 8. Enlargement of the $T > T_N$ region, showing the susceptibility maxima at 210 K for $n = 2$ and at 228 K for $n = 1$. The vestige of a similar effect may be evidenced in the inflection point near 164 K in the $n = 3$ system.

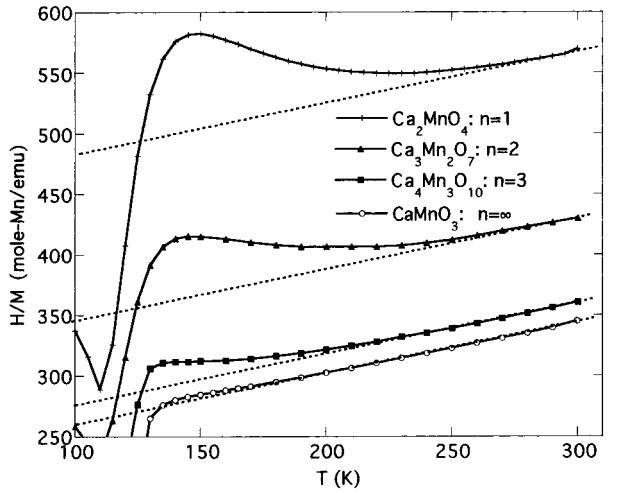

Figure 9. Inverse susceptibility $\chi^{-1} = H/M$. The dashed line though the high-T data of the $n = \infty$ system represents a CW relation with $\mu_{eff} = 2.60\ \mu_B$ and $\Theta = 511$ K. The dashed lines for the other curves represent a CW relation always with $\mu_{eff} = 2.60\ \mu_B$ but with $\Theta = 548$, 714, and 1037 K for the $n = 3$, 2, and 1 phases, respectively.

Structure. The Rietveld refinements show that there is a trend toward greater distortion in the MnO_6 octahedra with decreasing dimensionality (i.e. with decreasing value of n). The Rietveld fit of $CaMnO_3$ in this study yields similar results to those of the single-crystal structure published by Poeppelmeier et al.[20] The elongation of the apical Mn−O bonds in Ca_2MnO_4 has been noted before by Leonowicz et al.[21] although the difference between the apical and equatorial Mn−O distances was not as pronounced in their study. Leonowicz et al. also reported the neutron and X-ray powder structure determination of $Ca_2MnO_{3.5}$ in which, again, there are differences between the apical and equatorial Mn−O bond distances in the MnO_6 octahedra.[21] The Rietveld fit of the PXD data for $Ca_2MnO_{3.5}$ showed a distortion similar to the one noted in the Rietveld fit for Ca_2MnO_4 in this study (Table 6). Clearly, a distortion of this type would be expected in the $Ca_2MnO_{3.5}$ compound because the manganese valence is formally 3+ and thus it corresponds to a Jahn−Teller distorted d^4 ion. However, the Mn K-edge XAS spectrum of Ca_2MnO_4 clearly indicates that the manganese valence is at or close to 4+. A Mn^{3+} induced Jahn−Teller distortion measurable by X-ray diffraction would require a much higher concentration of Mn^{3+} than that which is observed. The lengthening of the apical Mn−O bond can then be attributed to the environment of the oxygen. The oxygen atom in the apical site is only bonded to a single manganese atom while the equatorial oxygen atoms are bonded to two manganese atoms. The lengthening of the apical Mn−O bonds will also lead to a splitting of the t_{2g} orbitals with the d_{xz} and d_{yz} orbitals being stabilized relative to the d_{xy} orbitals, which leads to a lowering of the electronic energy for the d^3 configuration.

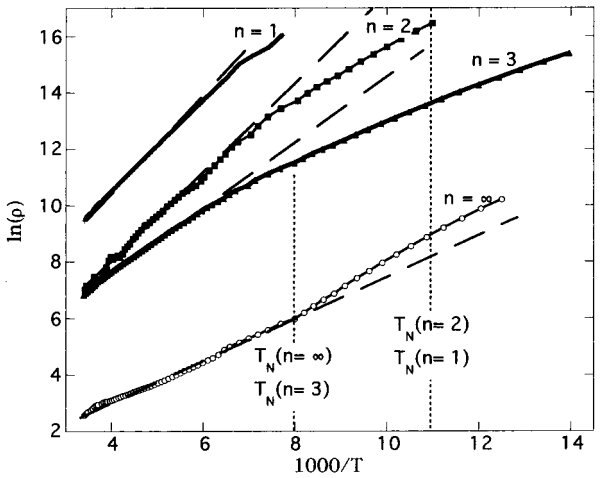

Figure 10. $\ln(\rho)$ vs reciprocal temperature for $(CaO)(CaMnO_3)_n$ ($n = 1$, 2, 3, and ∞).

Table 7. High-Temperature Fit of the Data to the Activated, $\rho(T) = \rho_0 \exp[\Delta/T]$, Form

RP phase	Δ (K)[a]	ρ_{RT} (Ω cm)	ρ_0 (Ω cm)
Ca_2MnO_4	1620 (0.14)	1.1×10^4	55
$Ca_3Mn_2O_7$	1550 (0.134)	1.3×10^3	6.0
$Ca_4Mn_3O_{10}$	1120 (0.0966)	8.32×10^2	23
$CaMnO_3$	717 (0.0618)	12.3	1.2

[a] Values in parentheses are given in units of eV.

The Rietveld analyses of the $n = 2$ and 3 members of the RP series were complicated by *hkl*-dependent peak broadening. This indicates that there are defects in these compounds that need further investigation. However, our structural study using powder X-ray diffraction shows that the trend in the distortion of the MnO_6 octahedra found in Ca_2MnO_4 is continued. The lengthening of the apical Mn−O distances is most pronounced at the edge of the perovskite-like $(CaMnO_3)_n$ slabs neighboring the rock-salt-like CaO layers. In $Ca_3Mn_2O_7$, the apical Mn−O(3) bond (2.09 Å) which is directed into the CaO rock-salt-like layer is longer than the apical Mn−O(1) bond (1.918 Å) which is directed into the center of the perovskite-like $(CaMnO_3)_n$ slab (Table 6). For $Ca_4Mn_3O_{10}$ the Mn(2)−O(2) bond (directed into the CaO layer) is longer than the other Mn(2)−O bonds. Conversely, the Mn−O bond lengths in the MnO_6 octahedra at the center of the 3-layer perovskite-like slabs are all essentially equal (d(Mn−O) = 1.84(3) Å ×2, 1.87(5) Å ×2, 1.90(6) Å ×2) (Table 6). One reason for the distortion in the MnO_6 octahedra is due to the bonding requirements of oxygen. Within the

perovskite-like slabs, the oxygen atoms are shared between two manganese atoms, whereas at the edge of the slabs the oxygen atoms are only joined to one manganese atom. The results from our refinement for $Ca_4Mn_3O_{10}$ are in agreement with Battle et al.[14] apart from the anomalous Mn(2)−O(2) bond length of 2.42(2) Å. Battle et al.[14] obtained Mn(2)−O(2) distances of 1.95-(1) and 1.891(5) Å from X-ray diffraction and neutron diffraction data, respectively. However, as noted above, the propensity to form longer Mn−O bonds neighboring the rock-salt-like CaO layer is found also in the $n = 1$ and 2 members of the RP phases. The discrepancies between the two studies may be attributed to differences in sample preparation and to our relatively poor X-ray diffraction data. The significantly different lattice parameters between our sample and that of Battle et al. (Table 1), particularly the much longer *c* axis of our sample, also suggests different stoichiometries and/or defect structures of the samples investigated. Further structural studies using electron microscopy to analyze defects combined with information on short-range order from EXAFS or neutron scattering are needed to investigate fully these trends.

XAS. In Figure 4, note (top) the strong chemical shift between the Mn^{3+}/Mn^{4+} perovskite material spectra ($LaMnO_3/CaMnO_3$) is consistent with a formal valance increase involving strong Mn-d-hole creation as was emphasized by Croft et al.[23] All of the Ca-based RP compounds (middle) manifest very similar chemical shifts consistent with a Mn-d count close to that of (top) $CaMnO_3$ and consistent with their identical 4+ formal Mn valence. The Mn K-edge spectra of the pure and 50% La substituted 214 compounds are seen at the bottom of the figure. The La substitution has clearly induced a strong chemical shift to lower energy consistent with the substituted electrons going dominantly into the Mn-d orbitals. The preedge feature, noted in the Mn K edge XAS in Figure 4, is related to transitions into Mn d/d-p-hybridized final states and its intensity variation is typically interpreted as scaling with the Mn-d hole count. In Figure 5, the preedge *a* features of the $LaMnO_3/CaMnO_3$ compounds and the Ca_2MnO_4/$LaCaMnO_4$ compounds are separately superimposed. The correlation of the preedge *a*-feature enhancement with the increasing Mn-d hole count (i.e., upon replacing La with Ca) has been discussed at length for the perovskite series by Croft et al.[23] The spectral changes upon substitution of La for Ca in the 214 compound are essentially the same as seen in the perovskite series. Therefore the preedge feature variation reinforces the interpretation that the La-doped electrons have strong Mn-d character. Closer inspection of the Ca_2MnO_4 spectrum in Figure 5 reveals a subtle low energy-shoulder in its a feature. An even more subtle similar structure in the $CaMnO_3$ a feature can also be discerned.

Since the preedge feature is due to transitions involving the empty 3d final states such preedge feature splittings have been conventionally interpreted in terms of 3d-state splittings. In TiO_2, for example, the Ti K preedge a feature exhibits a splitting which agrees very well with the $t_{2g}-e_g$ octahedral crystal field splitting (as well as manifesting an additional excitonic component).[24,25] Also in the $(Sr,La)_2FeO_4$ compounds the Fe K preedge exhibits a splitting attributed by Omata *et al.*[26] to the $t_{2g}-e_g$ splitting. And finally recent Mn K edge studies of $Li_xMn_2O_4$ batteries have manifested strong $t_{2g}-e_g$ preedge feature splittings.[27]

Within this interpretation, the a1−a2 splitting in Figure 6 evidences a d-state splitting of about 2.6 eV in Ca_2MnO_4 ($n = 1$). Presumably the gradual decrease of this splitting with increasing *n* is due to the progressive increase of dimensionality. Namely, for $n = 1$ the two apical oxygens are elongated toward the CaO layers relative to the equatorial oxygens. For the $n = 2$ material one of the apical oxygens is shared with another Mn site similar to the perovskite, while the other is bounded by a CaO layer. For the $n = 3$ material the central of the three Mn layers is bonded above and below like a perovskite with the CaO boundaries being removed to the adjoining Mn-apical positions and so on, until for $n = \infty$ all Mn−O bonds are equally shared. Thus in the octahedrally coordinated perovskite a $t_{2g}-e_g$ splitting is anticipated while in the $n = 1$ case an additional splitting should spread the d-states over a wider energy range with the other cases falling intermediate. This trend is consistent with the qualitative behavior observed in the a1−a2 splitting. The intensity variation in the a1 and a2 features, on the other hand, involves more subtle issues such as the degree of hybridized p (dipole allowed) character involved in these final states and will not be addressed here.

Magnetic Properties. In Figure 7 the magnetic susceptibility of the Ruddlesden−Popper (RP) phases $Ca_{n+1}Mn_nO_{3n+1}$ with $n = 1$, 2, 3, and ∞ show that the $n = \infty$ and $n = 3$ compounds spontaneously order both at ∼125 K, in good agreement with previous work.[12−14] Both the $n = \infty$ and 3 compounds are known to order in a simple G-type antiferromagnetic (AF) structure.[8,14] The small ferromagnetic moment exhibited below the AF ordering temperature for the $n = \infty$ and $n = 3$ compounds is due to spin canting in the AF phase in the external field. The low-field AC susceptibility work of Rossell et al. manifested a sharp peak at the antiferromagnetic transition (T_N) for the $n = 3$ compound[13] as did the zero-field cooled low-field susceptibility of Battle et al.[14] Thus the disparity between these low-field results and our 15 000 G results mandates that the spin canting in the $n = 3$ AF phase at least is nonlinear.

The $n = 1$ and 2 susceptibilities exhibit strong maxima at about 110 K which are assigned as their approximate T_N. These ordering temperatures are consistent with previous work.[12,28] It is worth noting that the failure of the magnetic ordering temperature to decrease with decreasing dimensionality from $n = \infty$ (3D) to $n = 1$ (2D) was the central point of the original work by MacChesney et al.[12]

(23) Croft, M.; Sills, D.; Greenblatt, M.; Lee, C.; Cheong, C.; Ramanujachary K. V.; Tran, D. *Phys. Rev.* **1997**, *B55* (14), 8726.

(24) Poumellec, B.; Cortes, R.; Tourillon G.; Berthon, J. *Phys. Stat. Sol.* **1991**, *164*, 319.

(25) Uozumi, T.; Okada, K.; Kotani, A.; Durmeyer, O.; Kappler, J. P.; Beaurepaire, E.; Perlebas, J. C. *Europhys. Lett.* **1992**, *18*, 85.

(26) Omata, T.; Ueda, K.; Hosono, H.; Katada, M.; Ueda, N.; Kawazoe, H. *Phys. Rev.* **1994**, *B49*, 10, 194.

(27) Croft, M.; Bates, J. Unpublished results.

(28) Cox, D. E.; Shirane, G.; Birgenau, R. J.; MacChesney, J. B. *Phys. Rev.* **1969**, *188* (2), 930.

Previous authors have commented on the unusual, nearly temperature independent magnetic susceptibility (for $T > T_N$) for the $n = 1$ material.[29,30] However previous work has failed to present the magnetic results for all of these materials in a consistent emu/mol of Mn form so that their magnetism could be compared directly. This has been done in Figure 7, which clearly emphasizes that there is a systematic and large overall depression of the Mn-magnetic response, in the $T > T_N$ range, with decreasing n. The expected mean field CW susceptibility for full-local-moment Mn^{4+} (μ_{eff}(full) = 3.87 μ_B) with $\Theta = T_N = 125$ K is also displayed in Figure 7. Figure 7 dramatically underscores that the Mn-magnetic response, even in the pure 3D perovskite, is substantially suppressed with respect to simple local moment behavior, a point that seems to have escaped comment in the previous work.

In Figure 8 (the expanded view of the $T > T_N$ range from Figure 7) the presence of subtle maxima in the χs of the $n = 1$ and $n = 2$ compounds, well above their ordering temperatures, is clearly visible. Indeed a flattening in the susceptibility of the $n = 3$ compound, very close to T_N, is suggestive of a vestigial maximum. Since the canting yields a small FM signature at the transition such a deviation from a monotonically increasing slope just above T_N is not expected. The susceptibility maximum in the $n = 1$ compound was noted in the measurements of Davis (as cited in ref 12 and again in the paper by Lines[30]). This maximum was attributed to short-range fluctuations at temperatures well above the ordering temperature in this $n = 1$, 2D layered material.[30] More recently quasi-2D magnetic fluctuations above T_N (after the interpretation of Lines) have been invoked for the $n = 3$ system.[14]

Goodenough discussed the nearly temperature independent susceptibility of the $n = 1$, 2, and 3 materials and speculated that these Mn compounds were close to the critical covalency strength for the crossover from local-moment behavior to itinerant moment behavior. He cited the CW behavior of the $n = \infty$ as evidence for local moment behavior in the parent 3D perovskite.[29]

To address the CW character (or more precisely its absence) in our measurements we present in Figure 9 plots of the inverse susceptibility versus temperature for all of the compounds measured. The dashed line passing through the $n = \infty$, high-T data represents the relation $\mu_{eff} = 4.34\ \mu_B$ and $\Theta = 511$ K. The full moment for Mn^{4+} is $\mu_{eff} = 3.87\ \mu_B$, and the reported ordered phase moment (for the $n = \infty$ compound) lies in the range 2.4−2.6 μ_B so that the CW moment is apparently an artifact of basically non-CW behavior. The Θ value of 511 K is clearly anomalously high for a material with $T_N = 125$ K as was underscored in Figure 7.

The $n = 3$ compound clearly has a more limited CW region, and the dashed line tangent to the high-T data represents a CW relation where $\mu = 4.34\ \mu B$ has been fixed and $\Theta = 548$ K is found. The unrealistically high Θ in this material was pointed out in ref 14 and attributed to 2D fluctuations. It should be noted that Battle et al. did not perform measurements on the 3D $n = \infty$ material, for which our work shows a comparable (very high) Θ. Thus the purely 2D fluctuation interpretation for the high Θ is questionable.

The $n = 2$ and $n = 1$ compounds essentially show no region of CW behavior in the temperature range considered. The high-T approach to the CW curves with $\mu_{eff} = 4.34\ \mu B$ and $\Theta = 714$ and 1037 K, respectively, is illustrated by the dashed lines in Figure 9. The successively higher temperature at which the χ^{-1} curves peal away from the CW straight-dashed lines and the large vertical displacement with decreasing n of the χ^{-1} curves reflect the systematically decreasing Mn-magnetic response with increasing n.

The interpretation that the 2D magnetic fluctuations increase as n decreases and as one approaches a single 2D Mn−O plane (in the $n = 1$ limit) would appear qualitatively consistent with the high-T magnetic evolution with increasing n. The substantial enhancement in the energy scale of these short-range interactions, with decreasing n, does however present a substantial theoretical challenge to this interpretation. More importantly our results emphasize that the 3D perovskite $CaMnO_3$ already has an anomalously high Θ and low magnetic response at high T. Moreover, our results indicate that the increase of the Θ, the suppression of the Mn-magnetic response, and appearance of a high-T susceptibility maximum all appear to grow continuously, with decreasing n, out of the magnetically anomalous 3D-perovskite parent.

Thus our data indicates that consideration of the suppression of magnetic response, previously noted in these Mn $n = 1$, 2, and 3 RP phases should be extended to the moment reduction in the parent 3D perovskite. The interpretation of 2D magnetic fluctuations, while reasonable as a partial explanation for this effect in the $n = 1$, 2, and 3 compounds, is not tenable in the 3D perovskite parent. Indeed the question whether the 2D fluctuations play an important role at all must be critically reexamined. Perhaps the suggestion by Goodenough[29] that covalency induced loss of local moment behavior or some similar method of moment reduction should be reconsidered. The role of frustration should also be considered, although nearest-neighbor AF interactions leading to type-G ordering in the 3D perovskite are not expected to be frustrated. The presence of Mn^{3+} sites, which would couple ferromagnetically to the Mn^{4+} sites, could be one source of a frustration suppression of the magnetic response; however, this should have introduced a FM reduction in Θ. Further work, both experimental and theoretical, is clearly required on these issues.

Electrical Resistivity. Figure 10 shows the ln(ρ) versus 1000/T for all of these RP manganates. The much larger resistivity of the $n < \infty$ materials is reasonably associated with the introduction of the insulating-CaO layers between the preovskite blocks. The increase in the resistivity as the thickness of the lower-resistivity perovskite block decreases (i.e. with decreasing n) is similarly reasonable. The detailed magnitude and temperature dependence of the resistivity of the $n = 2$ material appears, both from the figure and the fit parameters, to deviate somewhat from the systematic trend (Table 7). In view of potentially large anisotropy and intergrain effects, single-crystal results on these materials must be obtained before definitive conclusions can be drawn on these trends.

(29) Goodenough, J. *Phys. Rev.* **1967**, *164*, 785.
(30) Lines, E. *Phys. Rev.* **1967**, *164*, 736.

Regarding the temperature dependence of the resistivities, they clearly deviate from a simple single activation energy behavior. The long-dashed lines indicate the high-T-activated behavior, and the gap energies (Δ), determined by least-squares fitting the high-T data, are shown in Table 7. The resistivities of the $n < \infty$ materials all crossover to a weaker T-dependence at lower temperature. It should be noted that these resistivity crossovers for the $n = 3$ and $n = 2$ phases appear poorly or uncorrelated with the AF ordering temperatures. It is possible to obtain straight line plots of $\ln(\rho)$ versus $(T_o/T)^{\alpha}$, as might be expected from 3D ($\alpha = {}^1/_4$) or 2D ($\alpha = {}^1/_3$) localization; however, the T_o parameters are unrealistically large if a fit over the entire temperature range is attempted.[31] Thus at this juncture it appears reasonable to interpret the high-T resistivity as activated with the weaker lower-T resistivity being due to impurity carrier conduction, which will presumably show localization at much lower temperatures.

In contrast, the resistivity of the $n = \infty$ perovskite manifests a different temperature dependence. The high-T behavior appears activated; however, the low-T data deviate toward increased resistivity. Interestingly this deviation occurs close to the AF ordering temperature of the $n = \infty$ material and may be coupled to the AF order.

Conclusions

Ruddlesden−Popper (RP) phases, $Ca_{n+1}Mn_nO_{3n+1}$ with $n = 1$, 2, 3, and ∞, have been prepared using the Pechini citrate gel process at temperatures as low as 900 °C under flowing oxygen. Rietveld analysis indicates a systematic increase, with increasing $n = 1-3$, in the elongation of the Mn−O distances at the edge of the perovskite slab near the CaO rock-salt-like layers apparently associated with the oxygen environment. X-ray absorption near-edge spectroscopy results show unambiguously that Mn is formally 4+ in all these calcium-RP manganates. The magnetic susceptibility data show AF magnetic ordering in all the RP manganates in agreement with previous results.[12,14] However, the magnetic results shown in this work demonstrate for the first time that there is a systematic and large overall depression of the Mn-magnetic response, in the $T > T_N$ range, with decreasing n. The expected mean field CW susceptibility for full-local-moment Mn^{4+} even in the pure 3D perovskite is substantially suppressed. Thus 2D magnetic fluctuations, previously invoked to explain deviations from expected localized moment behavior in the $n = 1$ and 3 phases, are clearly not adequate.[30] The temperature dependence of the resistivities shows high-temperature activated behavior with a crossover to a weaker temperature dependence at lower temperature for the $n < \infty$ compounds. The $n = \infty$ perovskite manifests a much lower resistivity than the $n = 1$, 2, and 3 phases, consistent with the absence of insulating CaO rock salt layers. The increased resistivity near the AF transition may be coupled to the AF order in this material.

Acknowledgment. We thank Z. Zeng in our laboratory for providing the resistivity data for $CaMnO_3$ and Professor W. H. McCarroll for his critical reading of the manuscript and his many useful comments. This work was supported by the National Science Foundation Solid State Chemistry Grant DMR-96-13106. K.V.R. acknowledges funding from the Research Corp. Grant CC4366.

CM980380B

(31) Lien, N.; Rosenbaum, R. *Phys. Rev.* **1997**, *B56*, 14960.